Check for updates

ENVIRONMENTAL STUDIES

The large role of declining atmospheric sulfate deposition and rising CO_2 concentrations in stimulating future wetland CH_4 emissions

Lu Shen[1,2]*, Shushi Peng[3], Zhen Zhang[4], Chuan Tong[5], Jintai Lin[1], Yang Li[6], Huiru Zhong[1], Shuang Ma[7,8], Minghao Zhuang[9], Vincent Gauci[10,11,12]

Copyright © 2025 The Authors, some rights reserved; exclusive licensee American Association for the Advancement of Science. No claim to original U.S. Government Works. Distributed under a Creative Commons Attribution NonCommercial License 4.0 (CC BY-NC).

Existing projections of wetland methane emissions usually neglect feedbacks from global biogeochemical cycles. Using data-driven approaches, we estimate wetland methane emissions from 2000 to 2100, considering effects of meteorological changes and biogeochemical feedbacks from atmospheric sulfate deposition and CO_2 fertilization. In low-CO_2 scenarios (1.5° and 2°C warming pathways), the suppressive effect of sulfate deposition on wetland methane emissions largely diminishes by 2100 due to clean air policies, with resulting emission increases (7 ± 2 Tg a^{-1}) being 35 and 22% of total wetland emission changes. In mid-CO_2 scenarios (2.4° to 3.6°C warming pathways), sulfate deposition changes modestly, and CO_2 fertilization contributes >30% of wetland emission increases. Across all scenarios, biogeochemical feedbacks can stimulate 30 to 45% of future wetland emission rises. Under 1.5° and 2°C pathways, wetland methane emissions will likely increase by 20 to 34 Tg a^{-1} by 2100, representing 8 to 15% of the allowable space for anthropogenic methane emissions, a factor not yet considered by current assessments.

INTRODUCTION

Atmospheric methane (CH_4) is a potent greenhouse gas, which has been responsible for 0.6°C global warming since preindustrial times (*1*). Natural wetlands are the largest individual source contributing 120 to 210 Tg of methane annually as the result of anaerobic microbial decomposition of organic matter [90% confidence intervals (CIs), data S1], accounting for 20 to 40% of the global emission budget (*2*–*5*). The negative isotopic shift of $\delta^{13}C_{CH4}$ implies that the renewed methane growth after 2007 is likely caused by increases in microbial emissions, particularly from wetland methane feedbacks (*6*–*9*). The exceptionally high growth in atmospheric methane concentrations of 2020 and 2021 was also linked to intensified wetland emissions (*8*, *10*–*14*). In the past decade, the growth in field experiments has shown that wetland methane emissions should be closely linked to long-term changes in meteorology (e.g., temperature and precipitation) (*15*) and biogeochemical feedbacks (e.g., CO_2 enrichment and suppressive effects of sulfate deposition) (*16*, *17*). To date, few studies have sought to quantify future wetland methane emissions associated with the meteorological feedback (*18*–*24*), along with further evaluation of the biogeochemical feedback regarding CO_2 enrichment (*19*, *20*, *24*), in combination. Current Integrated Assessment Models, which design and evaluate mitigation pathways, do not directly incorporate future changes of wetland methane emissions (*25*).

Wetland CH_4 production is known to depend on climate, with increasing temperature and precipitation expected to stimulate methane emissions (*19*). Higher temperatures can facilitate microbial methanogenesis, increase substrate availability, and cause permafrost thawing, thus resulting in greater CH_4 production in wetlands (*15*, *26*–*30*). Increased precipitation can expand inundation extents, thereby rising methane emissions (*18*). In particular, there are still substantial uncertainties in parameterizing meteorological dependences of CH_4 emissions in process-based biogeochemical models (*27*, *31*–*34*), which hinders an accurate prediction of their responses to climate change. By the end of this century, previous studies projected an increase of wetland CH_4 emissions by 40 to 270 Tg a^{-1} in the "worst-case" [Representative Concentration Pathway 8.5 (RCP8.5) or equivalent] scenario (*22*–*24*, *35*) and by 14 to 50 Tg a^{-1} in a low-CO_2 scenario (RCP2.6 or equivalent) (*18*, *19*), which are highly uncertain.

Disturbances to wetland biogeochemistry, which have not yet been adequately assessed, could lead to large uncertainty in the estimated wetland methane emissions. Site-scale field experiments have demonstrated that atmospheric sulfate deposition can substantially suppress CH_4 emissions from natural wetlands by as much as 40% (*16*). This is because sulfate can stimulate the growth of sulfate-reducing bacteria, which outcompete methane-producing archaea for the same substrates (*36*, *37*). With sulfur emissions increasing substantially in the late 1990s, previous studies in the early 21st century predicted this suppressive effect to strengthen by the end of this century, thus offsetting warming-induced increases in wetland methane emissions (*16*). However, the projected decline of anthropogenic sulfur emissions by 2100 (*38*) implies that this conclusion needs to be revisited. Nitrogen deposition more likely stimulates methane emissions in natural wetlands by enhancing carbon substrates and methanogenic activities (*39*, *40*), but the magnitude of its influence on future wetland methane emissions is likely to be controversial (*39*–*41*) and is complicated by runoff of nitrogen fertilizers from nearby

[1]Department of Atmospheric and Oceanic Sciences, School of Physics, Peking University, Beijing 100871, China. [2]Institute of Carbon Neutrality, Peking University, Beijing 100871, China. [3]Sino-French Institute for Earth System Science, College of Urban and Environmental Sciences, Peking University, Beijing 100871, China. [4]Earth System Science Interdisciplinary Center, University of Maryland, College Park, MD 20740, USA. [5]Key Laboratory of Humid Subtropical Eco-Geographical Process, Ministry of Education, Fujian Normal University, Fuzhou 350007, China. [6]Department of Environmental Science, Baylor University, Waco, TX 76798, USA. [7]Joint Institute for Regional Earth System Science and Engineering, University of California, Los Angeles, Los Angeles, CA 90095, USA. [8]Jet Propulsion Laboratory, California Institute of Technology, Pasadena, CA 91011, USA. [9]College of Resources and Environmental Sciences, China Agricultural University, Beijing, 100193, China. [10]School of Geography, Earth and Environmental Sciences, University of Birmingham, Birmingham B15 2TT, UK. [11]Birmingham Institute of Forest Research (BIFoR), University of Birmingham, Birmingham B15 2TT, UK. [12]Birmingham Institute for Sustainability and Climate Action (BISCA), University of Birmingham, Birmingham B15 2TT, UK.
*Corresponding author. Email: lshen@pku.edu.cn

Downloaded from https://www.science.org at Peking University on February 11, 2025

cropland especially in northern boreal areas, Africa and upper Amazonia (*8*). On the other hand, the effects of rising atmospheric CO_2 on wetland CH_4 emissions remain largely ambiguous: It stimulates CH_4 production by increasing soil carbon availability (*17*, *42*) but decreases CH_4 emissions because of enhanced oxidation due to more oxygen supplied by plant roots (*43*, *44*). From paleoclimate records, the strong correlation between $\delta^{13}C_{CH4}$ and CO_2 concentrations implies that CO_2 fertilization was an important active feedback on wetland methane emissions, especially for C3 plants (*8*, *45*). However, to our knowledge, only simplified CO_2 fertilization mechanisms (e.g., stimulate vegetation production and soil carbon availability) have been included in present-day biogeochemical models (*10*, *19*, *24*). Nevertheless, the wealth of field experiments in recent years has substantially enriched our knowledge of these biogeochemical effects on methane emissions at the site scale, which we will synthesize here for a better and more accurate global estimate.

RESULTS

Overview of our approach and wetland emission baselines

We present a cross-disciplinary approach for extrapolating methane emissions into the future, building on a suite of empirical datasets and modeling results to constrain meteorological and biogeochemical feedback effects (Fig. 1). To model the meteorological feedback, we develop a regression model that considers both local and regional meteorological effects on wetland methane emissions, trained by wetland methane fluxes from 31 process-based inventories and 8 atmospheric inversions (table S1, text S1, and figs. S1 to S5). This regression model directly simulates the apparent sensitivity to meteorology, thus including confounding effects from other environmental and ecological factors. We apply this model to climate projections from an ensemble of Shared Socioeconomic Pathway (SSP) and RCP scenarios (39 climate models, 423 realizations, and seven climate scenarios) from 1900 to 2100 (table S2). To quantify the biogeochemical feedbacks, we compile available field measurements of methane fluxes in response to sulfate deposition and CO_2 enrichment (data S2 and S3), most of which are located in Northern Hemisphere. These empirical relationships are applied to deposition rates of sulfate, which are simulated by climate-chemistry models that participate in the Aerosol Chemistry Model Intercomparison Project (AerChemMIP) (4 to 10 models) (table S3) (*46*), and to future atmospheric CO_2 concentrations (*47*, *48*). Throughout this study, the uncertainties are expressed as 90% CIs from a Monte Carlo analysis, which considers errors arising from biogeochemical feedback pathways, empirical models trained by different wetland inventories, and meteorology projections from different CMIP6 models.

We determine the baseline of wetland methane emissions by collecting estimates from recently published data, in the context of their reporting periods dating back to the 2000s and using either bottom-up or top-down approaches. The bottom-up approach usually uses process-based biogeochemical models (*49*, *50*), and they report increasing trends between 2000 and 2019 (fig. S6). The top-down approach attributes the variability of in situ and satellite CH_4 concentrations to surface fluxes (*11*, *13*, *51*), by applying weight to prior guesses (usually from prior inventories) with observations. Thus, it can provide a unique opportunity to validate emission inventories where observations are abundant. Overall, wetland methane emissions from 2000 to 2019 are estimated to be 174 ± 45 Tg a^{-1} (90% CI) from 135 studies, with similar magnitudes between bottom-up (173 ± 55 Tg a^{-1}, $n = 74$) and top-down (175 ± 29 Tg a^{-1}, $n = 61$) approaches (fig. S7 and data S1). The high uncertainty from bottom-up methods is linked to the inadequate representations of abiotic inputs [e.g., the inundation extent (*52*, *53*) and water table depths (*54*)], as well as the complexity of the parameterizations in methane biotic processes (*30*, *49*, *55*) and egress pathways (*56*). For example, measured methane emissions in Zambian wetlands were an order of magnitude higher than those simulated by land surface models (*57*). Top-down approaches can reduce some of these uncertainties, although these assessments cannot rule out the biases resulting from incomplete coverage of observations, modeled atmospheric transport,

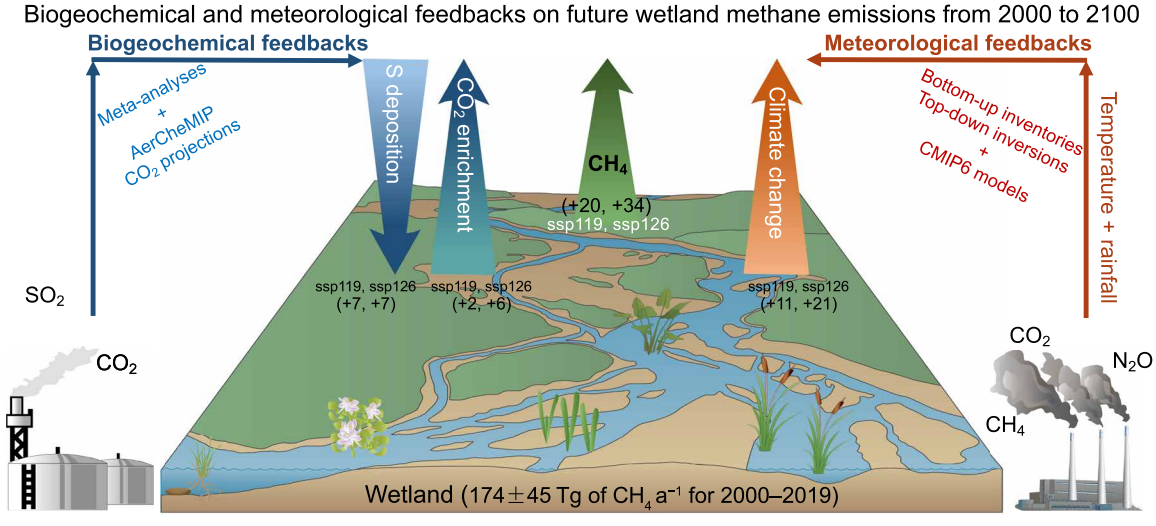


Fig. 1. Our data-driven framework to evaluate future wetland methane emissions. This work evaluates the combined effects of biogeochemical and meteorological feedbacks on wetland methane emissions. The numbers in the parenthesis denote methane emission changes (not absolute emissions) from 2000 to 2100 for two mitigation scenarios (ssp119 and ssp126) targeting 1.5° and 2°C goals, with contributions by two feedback pathway effects.The icons used in this figure are from Integration and Application Network (ian.umces.edu/media-library) under Attribution-ShareAlike 4.0 International (CC BY-SA 4.0).

Downloaded from https://www.science.org at Peking University on February 11, 2025

observation sources (*4*) (e.g., satellite and isotope), flux partitioning (*51*), and the uncertainties in wetland extents used in the inversion system.

Biogeochemical sensitivities to sulfate deposition and CO_2 enrichment

Figure 2A reveals an emergent pattern of increasing suppression of wetland methane emissions with increasing sulfate deposition up to 40 kg of S ha^{-2} a^{-1}. This empirical relationship is based on collected data from 30 independent field and controlled environment experiments (data S2). These suppressive relationships are consistent with what Gauci *et al.* (*16*) found from 15 measurements. These suppression effects arise from sulfate-reducing bacteria, which can outcompete methanogens for substrates and use sulfate as a terminal electron acceptor for the degradation of organic compounds (text S2) (*16*, *58*), thereby mitigating the production of methane. The suppression effect substantially increases with sulfate deposition rates less than 40 kg of S ha^{-2} a^{-1}, and then it reaches a saturation state (~40%) for larger rates (Fig. 2A). This saturation effect arises likely due to the confounding presence of other factors (substrate availability and temperature), which become the limiting factors rather than sulfate supply.

Because sulfur pollution is expected to decrease considerably in response to global efforts in curbing air pollution and acid rain (fig. S8A) (*38*), it is important to examine how it may alter wetland methane emissions. Figure 2B displays the amount of sulfate deposited on wetlands from 1900 to 2100 in historical and different future trajectories (*38*). The peak time of sulfate deposition is in the 1980s at the global scale (Fig. 2B), mainly driven by the peak of anthropogenic SO_2 emissions in North America and Europe (fig. S9) in the same period. Emissions in China and South Africa peaked in the 2010s and are projected to decrease in the future in all scenarios. However, in many other developing regions including India, Africa, Middle East, South America, and Southeast Asia, future changes of anthropogenic SO_2 emissions highly depend on socioeconomic scenarios (fig. S9). In the cleanest ssp119 scenarios with strong clean air policies, sulfate deposition on wetlands will return to the 1900 level after 2050, implying higher methane emissions due to alleviated

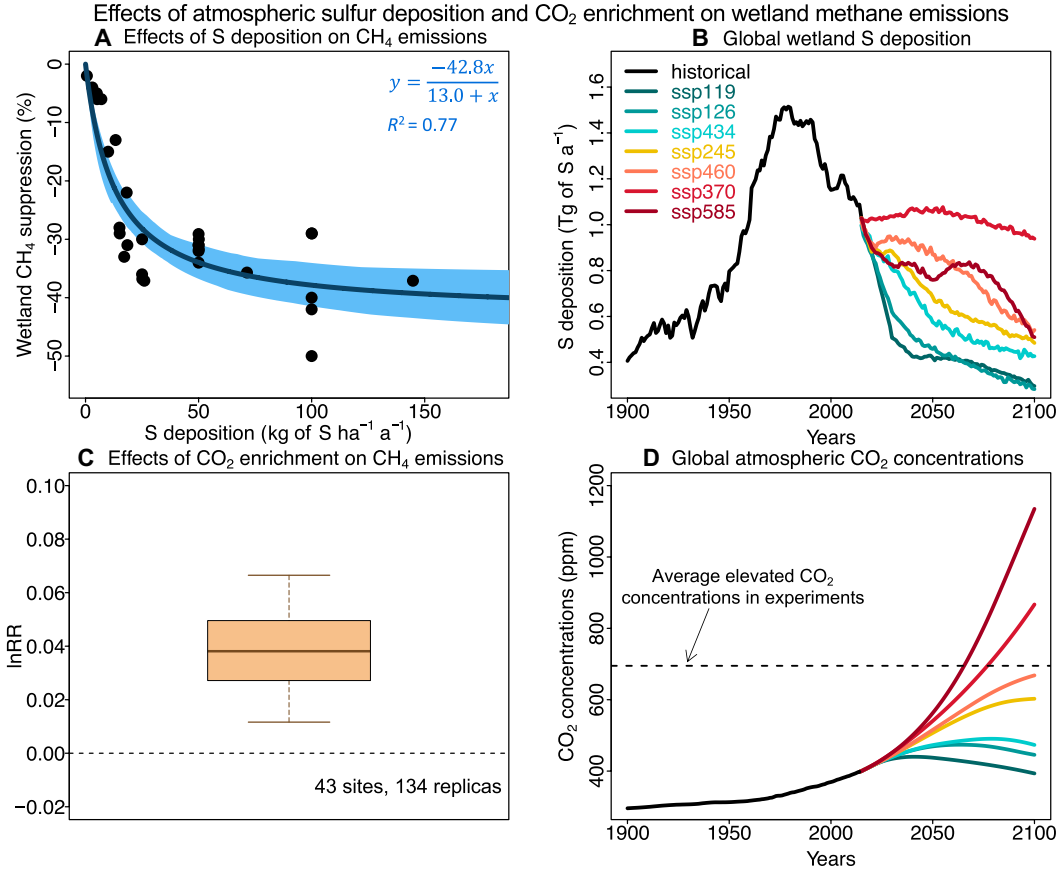


Fig. 2. Effects of atmospheric sulfate deposition and CO_2 fertilization on wetland methane emissions. (**A**) Suppressive effects of sulfate deposition on wetland methane emissions (data S2). Shaded area denotes the 90% CIs of fitted relationships from 1000 bootstrap experiments. (**B**) Global wetland sulfate deposition from 1900 to 2100 along different climate and socioeconomic pathways, calculated from Aerosol Chemistry Model Intercomparison Project (AerChemMIP) models. The global wetland area is from Wetland Area and Dynamics for Methane Modeling (*82*). (**C**) The natural log of global mean response ratio (lnRR), which describes the sensitivity of wetland methane emissions to per 100–part-per-million (ppm) increase of atmospheric CO_2 concentrations collected from published studies. The mean lnRR is obtained from randomly selecting samples from observations (data S3), weighted by replication of each experiment, using a Monto Carlo method. The hinges in boxplots refer to the 5th, 25th, 50th, 75th, and 95th quantiles. (**D**) Global mean atmospheric CO_2 concentrations (*48*) from 1900 to 2100 in seven future scenarios. The dashed line denotes the average elevated CO_2 concentrations in CO_2 fertilization experiments (data S3).

Downloaded from https://www.science.org at Peking University on February 11, 2025

sulfate suppression. In more polluted ssp370 scenarios, sulfate deposition will remain at 70% of the 1980s' level globally by the end of this century and increase in tropical areas where large wetland areas are located (fig. S8).

We assess the response of wetland methane emissions to CO_2 enrichment by compiling published experimental data from 43 field sites from published literature (data S3), which encompass a wide range of wetland ecosystem types. These experiments, primarily conducted in northern mid- to high-latitude wetlands, typically elevated CO_2 concentrations from 300 to 400 parts per million (ppm) to 600 to 800 ppm (data S3). Overall, we identify positive responses of wetland methane emissions to rising CO_2 concentrations, and the magnitude does not show a notable dependence on wetland types or water table levels (fig. S10), although controlled environment CO_2 manipulation experiments do suggest a nutrient status contingency on wetland methane emission responses to variable CO_2 concentrations (*59*). We use the mean value of all experimental data to upscale the global total and apply it to future climate scenarios. On the basis of this dataset, increased CO_2 stimulates CH_4 emissions from natural wetlands at an exponential rate of 0.038% (0.01 to 0.067%) ppm^{-1} (Fig. 2C). C4 plants are less responsive to elevated CO_2 concentrations (*8*, *60*, *61*); thus, later, we include a sensitivity test by excluding C4-dominated wetlands (fig. S11) (*62*) from our calculation of CO_2 fertilization effects while retaining them in the calculations of meteorological effects (temperature and precipitation) and sulfate suppression. However, our understanding of the latitudinal distribution of C4 vegetation and its response to CO_2 fertilization still remain limited, as these factors are not adequately constrained by current observations. Figure 2D shows the changes in CO_2 concentrations under different climate scenarios (*47*, *48*). In 2000, the global mean CO_2 concentration was 370 ppm. By 2100, CO_2 levels will be 390 ppm after an overshoot to 440 ppm around 2050 in ssp119 or almost triple (~1150 ppm) in the extreme warming scenario ssp585.

Future wetland CH_4 emissions and attribution to different driving factors

Our objective is to assess the share between meteorological and biogeochemical (sulfate suppressive effect and CO_2 fertilization) feedback effects in the projected trajectories of natural wetland methane emissions using our empirical models (Fig. 3) in different radiative forcing and socioeconomic scenarios (Fig. 4), as predicted by CMIP6. However, projections to extreme warming scenarios (ssp370 and ssp585) by 2100 are subject to very high uncertainties for three reasons. First, CO_2 levels in these two scenarios will far exceed (by up to 50%) the concentration range of CO_2 fertilization experiments (Fig. 2D), making the extrapolation of fertilization effects to 2100 highly uncertain. Second, the effects of CH_4 released from permafrost thawing are not well represented in CMIP6 models (*25*, *63*) and, thus, cannot be accurately quantified in this work. Third, plants are expected to adapt to warming environment, e.g., the evolution of C3 and C4 plant distribution in a warmer climate (*64*, *65*), which is difficult to accurately characterize (*18*). Thus, we only display future changes regarding these low- to mid-CO_2 scenarios in the main text, and the results about high-CO_2 climate scenarios are in the Supplementary Materials.

As shown in Fig. 3A, over the 1900–2000 period, wetland emissions remain relatively stable, and the lowest emissions are around the 1980s partly due to the peaking suppressive effects from anthropogenic sulfur emissions (Fig. 3B and fig. S12). The influence of meteorology and CO_2 fertilization becomes evident since 2000, stimulating much faster increase of methane emissions than in the 20th century (Fig. 3B), consistent with previous work (*10*, *19*). Our results show that mean global CH_4 emissions from natural wetlands

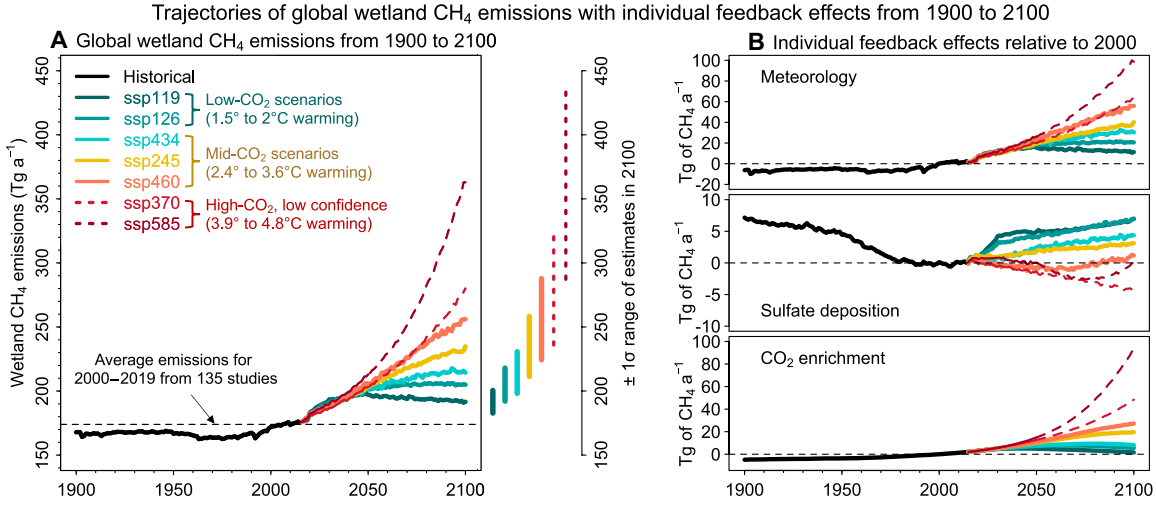


Fig. 3. Global wetland methane emissions from 1900 to 2100 with contributions from individual feedback effects. (**A**) Global wetland CH_4 emissions from 1900 to 2100 in historical and seven future scenarios. The right panel of (A) shows the range of ±1σ for the emissions at the end of the 21st century. The horizontal line denotes the average emissions over the 2000–2019 period (174 Tg a^{-1}) collected from 135 studies (data S1). For the two high-CO_2 scenarios, ssp370 and ssp585, the projections are subject to large uncertainty because of extreme extrapolations of CO_2 fertilization effects and underrepresentation of mechanisms like permafrost thawing and plant adaptation in CMIP6 models and, thus, denoted as dashed lines. The rises in global surface air temperature from 1850–1900 to 2081–2100 (*47*, *86*) under different climate scenarios are shown inset. (**B**) Individual feedback effects on wetland CH_4 emissions from meteorology, sulfate deposition, and CO_2 enrichment. All feedback effects are shown as changes relative to the year 2000 (171 Tg a^{-1}). Additional details on the contributions from each feedback pathway, along with the total emission trajectories on a decadal scale, can be found in fig. S13.

Downloaded from https://www.science.org at Peking University on February 11, 2025

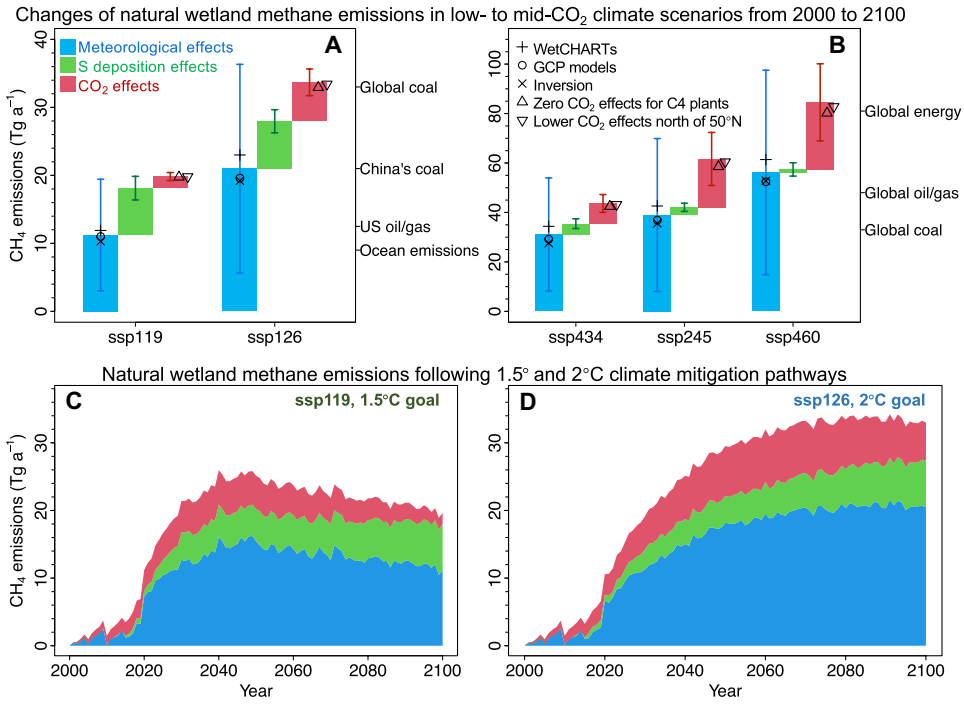


Fig. 4. Contributions of meteorological and biogeochemical feedbacks (CO_2 fertilization and sulfate suppressive effect) in wetland methane emission. The changes are calculated using as reference the year 2000. (**A** and **B**) Methane increases from meteorological feedback, sulfate deposition effects, and CO_2 enrichment in low- to mid-CO_2 scenarios from 2000 to 2100. On the right *y* axis of (A) and (B) shows the comparison with major global emissions from the ocean (*66*), the US oil/gas industry (*67*), China's coal (*68*), global oil/gas and coal industry (*68*), and global livestock (*3*). Calculated average meteorological effects based on inventories from WetCHARTs, GCP wetland models, and atmospheric inversions are shown inset (table S1). The upward triangles denote the CO_2 fertilization effects after excluding C4 plants in calculation. The downward triangles denote the calculated CO_2 feedback by lowering the response sensitivity of wetland fluxes north of 50°N (see fig. S21 for details). Detailed numbers of contribution from different feedback effects are displayed in table S4. (**C** and **D**) Time series of wetland methane emissions relative to the 2000 level for the two mitigation scenarios targeting 1.5° (C) and 2°C (D) goals, with the contribution of different driving factors included.

may increase from 171 Tg of CH_4 a^{-1} in 2000 by 20, 34, 44, 62, and 85 Tg of CH_4 a^{-1} in ssp119, ssp126, ssp434, ssp245, and ssp460, respectively, in 2100 (Fig. 3). In the strongest climate mitigation scenario (ssp119), wetland CH_4 emissions peak around the 2050s (~198 Tg of CH_4 a^{-1}) and decline slightly thereafter. In the two extreme warming scenarios, ssp370 and ssp585, wetland CH_4 emissions increase by 60 to 110% by the 2100s, with an increasing trend throughout the century but with very high uncertainty. The contribution of each feedback effect alongside total emissions on a decadal scale for all scenarios can be found in fig. S13.

In low-CO_2 scenarios (ssp119 and ssp126, 1.5 to °2°C warming pathways), climate warming and declining sulfate deposition are the primary drivers of increasing wetland methane emissions (Fig. 4A). In response to clean air policies, anthropogenic sulfur emissions are expected to return to the 1900 level by the 2100s (fig. S8), substantially alleviating their suppression effects on wetland methane formation. Such alleviating effects are most notable between 2020 and 2050 (fig. S8), during which period anthropogenic sulfur emissions decrease by ~50 Tg of SO_2 a^{-1} (or by ~70% relative to 2020). Consequently, the induced increase in methane emissions from 2000 to 2100 is 6.9 ± 1.8 Tg a^{-1} in ssp119 and 7.0 ± 1.8 Tg a^{-1} in ssp126, amounting to 61 and 33% of the wetland methane emissions from meteorological effects alone (temperature and precipitation effects, table S4). By 2100, methane increases from the ssp119 and ssp126 scenarios are estimated to be 20 and 34 Tg a^{-1}, respectively, and the biogeochemical feedback explains 43 and 38% of these increases. More specifically, in these two scenarios, CO_2 enrichment explains 9 and 17%, and decreasing sulfate deposition explains 35 and 21% of the total increase in methane emissions. These emission enhancements are 2.2 to 3.8 times global oceanic sources (9 Tg a^{-1}) (*66*), 1.6 to 2.7 times emissions from the oil-gas industry of the US (12.5 Tg a^{-1}) (*67*), and comparable to the emissions from China's coal (21 Tg a^{-1}) or global coal industry (33 Tg a^{-1}) (*68*). In the ssp126 scenario (equivalent to RCP2.6 in CMIP5), the emission increases resulting from meteorological and CO_2 feedbacks are 27 Tg a^{-1} in this study, which is in the range of 14 to 36 Tg a^{-1} [an exceptionally high projection of 50 Tg a^{-1} from Zhang *et al.* (*19*) is not considered here] from five previous estimates (table S5) (*10*, *18*, *20*, *21*, *24*). The meteorological feedback alone is expected to increase wetland emissions by 21 ± 4 Tg a^{-1}, higher than the estimate (14 Tg a^{-1}) of Koffi *et al.* (*18*) who accounted for plant adaption to rising temperatures using an empirical approach. However, after including the biogeochemical feedback from sulfate deposition, our estimated methane increases (34 Tg a^{-1}) in ssp126 are almost the highest of all studies in the low-CO_2 scenario (*18*, *24*).

In mid-CO_2 scenarios (ssp434, ssp245, and ssp460, 2.4° to 3.6°C warming pathways), climate warming and CO_2 enrichment are the primary drivers of amplifying wetland methane emissions by 44 to 85 Tg a^{-1} (Fig. 4B) in 2100 relative to 2000. In these scenarios, temperature and precipitation will experience substantial increases

Downloaded from https://www.science.org at Peking University on February 11, 2025

(figs. S14 and S15), promoting microbial activities and expanding wetland areas, especially in northern boreal regions (fig. S16). The estimated stimulations range from 31 to 56 Tg a^{-1} through meteorological feedback and 8 to 27 Tg a^{-1} through increased atmospheric CO_2 concentrations. The effects of sulfate deposition in driving future wetland methane emissions change relative to 2000 (1 to 5 Tg a^{-1}) are much less than those of other feedback pathways. If we assume that the C4-dominated wetlands (fig. S11) (*62*) are not responsive to elevated CO_2 concentrations (*60*, *61*), then the magnitude of CO_2 fertilization effects on wetland methane emissions will be lowered by 3.1 and 4.4 Tg a^{-1} (or ~16%) in 2100 relative to 2000 in ssp245 and ssp460. Overall, biogeochemical feedback, mainly arising from CO_2 enrichment, contributes 30 to 40% of the total methane emission increases in ssp434, ssp245, and ssp460, and 40 to 50% in ssp370 and ssp585 (table S4).

In reference to policy questions, anthropogenic emission needs to be mitigated by 180 Tg a^{-1} and 130 Tg a^{-1} toward the 1.5° and 2°C warming goal from 2020 to 2050 (*38*), respectively. On the basis of our assessment, wetland methane emissions will increase by 14 and 19 Tg a^{-1} along these two trajectories (Fig. 4, C and D) for the same period (table S6), amounting to 8 to 15% of the mitigation target, which has not been taken into account in present-day climate assessment. The Global Methane Pledge aims to reduce anthropogenic methane emissions by ~100 Tg a^{-1} (30%) from 2020 to 2030 (*69*); during this same period, wetlands emissions are estimated to increase by 10 Tg a^{-1} in ssp119 (Fig. 4, C and D, and table S6). These results suggest that achieving the 1.5° or 2°C warming goal needs 11 ± 4% more aggressive mitigation, which is lacking in the present-day climate assessment.

DISCUSSION

Our estimates of future emission paths are still hampered by the relative scarcity of reliable field manipulation experiments. For CO_2 fertilization effects, the response sensitivity calculated from these limited number of experiments has a high range (the relative SD is 30%), which results in highly uncertain projections of wetland methane emissions in these mid- to high-CO_2 scenarios (figs. S17 and S18). For example, in ssp245 and ssp460 scenarios, the difference of CO_2 fertilization effects from 2000 to 2100 can be 30 to 40 Tg a^{-1} between using the lower and upper bounds of CO_2 fertilization sensitivities (fig. S18). In addition, CO_2 concentrations were only elevated to 600 to 800 ppm in past field experiments (Fig. 2D), much lower than the expected 900 to 1150 ppm by 2100 in the two extreme warming scenarios (ssp370 and ssp585). For the suppressive effects of sulfate deposition, we assume that the response of wetland methane emissions is instantaneous and the suppressive effects from last year will not persist to the next year. This is supported by a field experiment showing that CH_4 emissions could return to baseline levels in 2 years if the sulfate deposition rate is less than 25 kg of S $ha^{-2}a^{-1}$ (*70*), and >90% wetlands in the future will be below half of this deposition rate. On the basis of field measurements from FLUXNET-CH4, we also find notably lower methane emissions in salted wetland ecosystems (e.g., salt marsh and mangrove), linked to the suppressive effects of high sulfate concentrations in the water environment (fig. S19). However, even after including observations dating back to the early 2000s, we still cannot find statistically significant evidence of increasing methane emissions that can be directly ascribed to declining atmospheric sulfate deposition. Detecting the effect of diminishing sulfate suppression amidst the highly variable flux data in FLUXNET-CH4 is challenging. This is because the interannual variability of wetland methane fluxes at the site scale (~25%) is influenced by a variety of environmental variables, such as temperature and water table depths, which cause far greater flux fluctuations than the effects of sulfate deposition (<5%) from 2000 to 2020. This disparity makes it difficult to isolate the impacts of sulfate deposition based on interannual observations (fig. S20).

Current field experiments regarding CO_2 fertilization effects are mainly conducted in northern mid- to high latitudes, raising a question whether these observed feedbacks are valid globally. Because it is not feasible to obtain additional experimental data from wetlands across all latitudes, we use process models to gain insights into this issue. Here, we examine the response sensitivity of wetland methane emissions in two land process model ORCHIDEE (*71*) and LPJ-wsl [Lund–Potsdam–Jena-Wald, Schnee and Landschaft; (*10*, *19*)]. Both models simulate similar magnitudes of CO_2 fertilization sensitivities across (sub)tropical and temperate wetlands (fig. S21). However, this consistency does not guarantee that these results hold valid in the tropics due to the lack of observations there. In north of 50°N, such a sensitivity slightly decreases in LPJ-wsl but substantially decreases in ORCHIDEE (fig. S21), because the influence of CO_2 on photosynthesis (the substrate for methanogens) at high latitudes is limited due to low temperatures (*72*). Thus, to simulate this declining CO_2 fertilization effects at higher latitudes, we conduct a sensitivity test assuming that the CO_2 fertilization effects of C3 plants gradually decline to zero from 50°N to 75°N (with minimal wetland presence north of 75°N). This adjustment results in a reduction in the magnitude of future changes in wetland methane emissions by <2 Tg a^{-1} in low- and mid-CO_2 scenarios (Fig. 4). Nevertheless, there is still substantial latitudinal variability in CO_2 fertilization effects across different process-based models (fig. S21) (*72*), which needs future investigation.

Current field experiments about the suppressive effects of sulfate deposition on natural wetlands are predominantly conducted in the mid- to high-latitude regions, whether these findings can be applied to lower latitudes remain unclear. However, similar reduction in methane emissions has been repeatedly observed in rice paddy agriculture experiments (*73*, *74*), which are a reasonable analog of natural wetlands across the tropics (fig. S22). These experiments conducted on rice paddies typically involve a single, high-dose application of sulfate, differing from natural wetlands that receive continuous, low dose of atmospheric deposition. This large single dose can therefore promote a more substantial inhibition (up to 70%, fig. S22) compared to the chronic, continuous low doses of sulfate in natural wetlands (Fig. 2A). Meanwhile, management interventions used in rice paddies, application of N-based fertilizers and incorporation of organic matter, would mitigate part of suppressive effect by sulfate because N fertilizers would have their own inhibitory effect and sulfate suppression relies on limited organic substrates over which competition with methanogens can occur (*73*). Despite these differences, the observed methane suppression by sulfate addition in rice paddies suggests that the interaction is as relevant in the tropics as it is in northern wetlands and would obey similar dose-response patterns.

Our framework is a data-driven approach that synthesizes results from recently published field measurements in combination with state-of-art modeling outputs. It may neglect some important

Downloaded from https://www.science.org at Peking University on February 11, 2025

physical mechanisms, especially those not yet being constrained by observations, including permafrost thawing (*25*), ecological adaptation to warming climate (*18*), the evolution of methanogen and methanotroph communities (*15*), nitrogen (*8*) and sulfate runoff from nearby anthropogenic sources (cropland and cities), and the limited understanding of wetland extent sensitivity to warming (*10*, *18*). The effects of atmospheric nitrogen deposition on wetland methane emissions is still controversial (*39*–*41*) and is complicated by runoff of nitrogen fertilizers from nearby cropland (*8*), which needs further investigation in the future. Net methane emissions represent the imbalance between microbial methane production (methanogenesis) and oxidation (methanotrophy), but the latter has been subject to far less investigation in previous studies (*15*) and is not well parameterized in biogeochemical models (*43*), which adds uncertainty to future projections. In high-CO_2 scenarios, wetland CH_4 emissions may act as positive feedback in amplifying the warming effects, which is not evaluated in this work. Because of the above reasons, our projections for extreme warming scenarios (ssp370 and ssp585) are subject to high uncertainties. Moreover, our empirical approach is designed in a way that it directly simulates the apparent sensitivity of wetland methane emissions to meteorological and biogeochemical factors. It cannot cancel out the confounding factors and their interaction if these factors influence methane fluxes distinctly in the future. This will introduce some uncertainty, which is difficult to quantify from field measurements.

In the context of climate change mitigation, future trajectories of wetland methane emissions under the lowest-CO_2 emission scenarios (ssp119 and ssp126) reduce the allowable space for anthropogenic methane emissions by 8 to 15%. This means that policy instruments such as the Global Methane Pledge will require steeper cuts to anthropogenic methane emission sources than stipulated if we are to stay within Paris Agreement guardrails of 1.5°C warming.

MATERIALS AND METHODS

Database 1: Wetland methane emissions from bottom-up and top-down approaches

Natural wetlands are defined as areas with soils permanently or temporarily covered by water, excluding those small ponds, rivers, and lakes. Here, we compiled peer-reviewed studies published before December 2022 using keywords including "wetland" and "methane emissions." Our efforts identified a total of 135 estimates from 100 publications (data S1), which use either bottom-up or top-down approaches. Results show that bottom-up (173 ± 55 Tg a^{-1}, 90% CI, $n = 74$) and top-down (176 ± 29 Tg a^{-1}, 90% CI, $n = 61$) approaches are consistent in magnitude. Synthesizing estimates from all studies, wetland methane emissions are determined to be 174 ± 45 Tg a^{-1} (90% CI) over the 2000–2019 period.

Database 2: Suppressive effects of sulfate deposition on wetland methane emissions

We extracted results for sulfate suppressive effects on wetland methane emissions using keywords including "sulfate" and "methane emissions" until December 2022. Our efforts identified a total of 30 experiments (data S2). Consistent with (*16*), we fit the observed suppression effects using the form of the Michaelis-Menten equation, which is written as

$$g(x) = \frac{ax}{b + x} \quad (1)$$

where $g(x)$ is the percent suppression of wetland methane emissions (%) and x is the sulfate deposition rate (kg of S ha^{-1} a^{-1}). a refers to the maximum of the suppressive effects and is optimized to be −42.8%, and b is 13.0 kg of S ha^{-1} a^{-1}. This empirical model is fitted to the available observations with a coefficient of determination (R^2) of 0.77.

Database 3: Effects of CO_2 enrichment on wetland CH_4 emissions

Responses of CH_4 emissions to atmospheric CO_2 concentrations were collected by searching for all peer-reviewed articles that were published before December 2022. For each study, we collected the coordinates of sites, wetland types, water table levels, ambient and elevated CO_2 concentrations, and methane fluxes. The final dataset (data S3) includes 118 experiments from 34 individual sites. These experiments increased atmospheric CO_2 concentration from 300 to 400 ppm to 600 to 800 ppm on average. We also examined whether any covariates, such as water table levels, latitudes, and ecosystem types, can explain the variability of the effect of increased CO_2, and none of such analyses is statistically significant (fig. S10).

Following (*17*), we use the natural log of the response ratio (lnRR) to assess the effect of CO_2 enrichment on methane fluxes from the wetland for each pair of data points

$$\mathrm{lnRR} = \frac{\ln\left(y_e / y_a\right)}{C_e - C_a} \quad (2)$$

where y is measured CH_4 flux under elevated (e) or ambient (a) CO_2 concentrations (denoted as C_e and C_a). We use the mean values of lnRR to upscale the global total and apply it to future climate scenarios.

In part of the work, we explore the response of wetland fluxes to CO_2 enrichments in two land surface models [ORCHIDEE (*71*) and LPJ-wsl (*10*, *19*)], aiming to examine the CO_2 fertilization effects at different latitudes and also verify our empirical results using these models. In ORCHIDEE, the methane scheme includes a detailed representation of methanogenesis from different carbon pools, oxidation and transport by plants, and ebullition and diffusion in soil (*75*). In LPJ-wsl, CH_4 emissions are modeled as a function of wetland extents, soil temperature, heterotrophic respiration, and an emitting factor empirically fitted to match latitudinal wetland CH_4 fluxes from an atmospheric inversion study (*10*, *19*). In both models, we perturb the ambient CO_2 concentrations by an increase of 200 to 300 ppm and maintain the meteorology at the present-day level, and the response sensitivity of wetland CH_4 emissions to CO_2 enrichment is displayed in fig. S21.

Wetland methane emissions from bottom-up inventories and top-down inversions

We examine present-day meteorological sensitivities of wetland methane emissions using methane fluxes from 31 bottom-up inventories and eight top-down inversions (table S1). For bottom-up estimates, we rely on 18 inventories from WetCHARTs v1.3.1 (*49*, *50*) and 13 land surface models that participate in the Global Carbon Project (GCP) (*3*). For top-down inversions, we use these inverted fluxes from Copernicus Atmosphere Monitoring Service and Monitoring Atmospheric Composition and Climate – Phase III (*76*). These estimates are produced using CH_4 concentrations from surface air measurements (discrete or in situ) or atmospheric CH_4 columns observed

Downloaded from https://www.science.org at Peking University on February 11, 2025

by satellites (*11*, *13*). These two top-down inversions use the same inversion scheme (*76*), so our results may underestimate the uncertainty arising from different settings in inversion methods.

Statistical models to describe current meteorological sensitivities of wetland methane emissions

We select surface air temperature (T) and precipitation (P) (*77*) as the key variables driving the monthly and interannual variability of wetland methane emissions, consistent with those in the previous studies (*18*). Overall, wetland methane emissions exhibit positive dependencies on P ubiquitously across the globe, positive dependence on T at high latitudes, but divergent correlations with T in the tropics (fig. S23). This is because the annual cycle of wet to dry seasons varies considerably in the tropics, making wetland methane emissions more sensitive to water limitations rather than temperatures, which are further modulated by large-scale ocean-atmosphere interactions (e.g., El Nino, La Nina, and India Ocean Dipole) (*8*, *78*, *79*).

Here, we consider local and regional meteorological effects in the model (text S1). The use of regional meteorological patterns can increase the model's predictive capability for two reasons. First, water moves across the earth's surface through runoff and streamflow; such spatial connections can be represented by satellite-constrained wetland extent but not necessarily by local meteorological factors (figs. S2 and S3). Second, local meteorology is usually subject to large bias in CMIP6 models due to inadequate representation of local terrestrial processes with a low spatial resolution (~100 to 200 km) (*80*), and regional climate patterns can be more accurate. Following (*81*), we construct regional climate patterns through the use of singular value decompositions (SVDs) of the spatial correlations between methane fluxes in each grid cell and meteorological variables (T and P) in grid boxes in the surrounding regions (1000 km). We do so for all the wetland grid cells across the globe, and the models are of two forms

$$E = a_1 T + a_2 P + \beta_1 S_1 + \beta_2 S_2 \quad (3)$$

$$\log(E) = a_1 T + a_2 \log(P) + \beta_1 S_1 + \beta_2 S_2 \quad (4)$$

where T and P refer to local temperature and precipitation, and S_1 and S_2 refer to regional climate patterns using the SVD. In each pixel, we fit the data with both models and select the one with a higher R^2. Overall, Eq. 4 is a better option at mid- to high latitudes, and Eq. 3 is used in the tropics where water limitation is a more determining factor in monthly variability (fig. S5). We find that local T and P and regional climate patterns (S_1 and S_2) collectively explained 70 to 90% of the variance in monthly wetland methane emissions, 20 to 30% higher than only using local meteorological variables (fig. S4).

Verification of the designed empirical models

We verify our empirical models with flux measurements from FLUXNET-CH4 and with the methane emission budget predicted by the Upscaling Wetland CH_4 (UpCH4) model. The UpCH4 is a six-predictor random forest model trained on 43 freshwater sites from FLUXNET-CH4, which then generates monthly, globally wetland methane emissions after taking into account wetland extents [e.g., Wetland Area and Dynamics for Methane Modeling; (*82*)]. According to McNico *et al.* (*83*), the UpCH4 product is subject to very high uncertainty in (sub)tropical regions due to observation scarcity (seven sites) and is more suitable for comparison in nontropical wetlands. At the site scale (fig. S24), the monthly temporal correlations of wetland methane fluxes between our empirical models and FLUXNET-CH4 data are 0.72 (90% CI, 0.05 to 0.89), and the ratios of annual mean flux rates are 0.98 (90% CI, 0.27 to 7.0). Outliers are attributed to the fact that our empirical models, trained at a 100-km horizontal resolution, may not accurately reflect the flux at the site location. When integrating fluxes by latitude bands, our designed empirical models show good consistency in total methane fluxes (fig. S25) and seasonality (fig. S26) with these observation-based datasets in nontropical regions, as well as with process-based models. We also verify the temperature dependence (Q10) in these Arctic-boreal and temperate wetland areas. In contrast, the temporal correlation of methane fluxes and surface air temperature is very low [correlation coefficient (r) < 0.2] in seven (sub)tropical sites, so the Q10 values are not calculated for these regions. In these nontropical areas, the Q10 metric of our empirical models is consistent with the observational estimates from FLUXNET-CH4 and UpCH4 (fig. S27).

Future projections of temperature and precipitation

Here, we select seven harmonized combinations of RCP and SSP scenarios (ssp119, ssp126, ssp245, ssp370, ssp434, ssp460, and ssp585), which encompass a wide range of radiative forcing values (1.9 to 8.5 W m^{-2}) and anthropogenic emission trajectories (table S2) (*84*). The quantile delta mapping (*85*) is applied to correct any systematic distributional biases in temperature and precipitation from CMIP6 models. In future scenarios, wetlands in mid- to high latitudes will become wetter and warmer; tropical wetlands are exposed to increasing T but to divergent trends in P. Meanwhile, northern high-latitude ecosystems are experiencing more rapid increases in temperature and precipitation than elsewhere (figs. S14 and S15). From 2000 to 2100, global wetland area (available in five CMIP6 models) remains largely unchanged (−3 to 5%) in low-CO_2 scenarios (ssp119 and ssp126) and increases by ~10% with large discrepancies across models (5 to 25%) in ssp585 (text S3 and figs. S28 and S29).

Future projections of atmospheric sulfur deposition and CO_2 concentrations

Future atmospheric deposition of sulfate is obtained from historical transient (1900 to 2014) and future (2015 to 2100) model simulations participating in AerChemMIP (table S3). These models include detailed tropospheric and stratospheric chemistry but may neglect some important processes like lateral nitrogen input into wetlands through runoff from nearly croplands (*8*). We use global monthly distributions of atmospheric CO_2 concentrations with 1° resolution under historical (1850 to 2013) and future (2015 to 2150) scenarios from Cheng *et al.* (*48*). The present-day CO_2 concentrations were 390 ppm in 2019 and will increase to 1150 ppm in ssp585 and to 390 ppm in ssp119 by the end of this century.

Estimate projections of wetland methane emissions in different scenarios

We combined current meteorological dependences and biogeochemical sensitivities with 1900–2100 projections of meteorology, S deposition, and CO_2 concentrations to generate wetland methane emissions. The final equation is written as

$$E_{\mathrm{month},i,j} = f\left(T_{\mathrm{month},i,j} P_{\mathrm{month},i,j}\right) \times g\left(S_{\mathrm{year},i,j}\right) \times h\left(\mathrm{co}_{2\mathrm{year},i,j}\right) \quad (5)$$

Downloaded from https://www.science.org at Peking University on February 11, 2025

$$h\left(CO_{2year,i,j}\right) = RR^{C_{year,i,j}-C_b} \quad (6)$$

where $E_{month,i,j}$ is methane emission in the (i, j)th grid cell in a specific month. $f\left(T_{month,i,j}, P_{month,i,j}\right)$ is estimated wetland emission on the basis of on $T$and Pusing statistical approaches (Eqs. 3 and 4). Because all inputs are at the monthly scale, thus already including the information of variability in wetland areas, we do not scale up our prediction using wetland area changes simulated by CMIP6 models. Future trends in wetland areas are driven by meteorological variables and, thus, can be represented by our model. For g and h, they refer to the relative changes to the observation period (2000 to 2019) for suppressive effects of sulfate deposition (Eq. 2) and CO_2 fertilization (Eq. 6). In Eq. 6, RR is the response ratio determined in Eq. 2, and C_b is the average CO_2 concentration during 2000 to 2019 (390 ppm).

Uncertainty assessment

To quantify the overall parametric uncertainty in projected trajectories of wetland methane fluxes, we conducted a Monte Carlo analysis by considering errors in each subprocess. (i) For the feedback effects of sulfate deposition and CO_2 fertilization, we estimate the range of response sensitivity from field experiments through bootstrap resampling. (ii) The empirical models, which assess the response to meteorology, are trained from 39 wetland inventories. (iii) Future projections of meteorology are obtained from different climate models, and the number of models varies across climate scenarios. Throughout this work, the uncertainty is reported as the 90% CI.

Figures S17 and S18 further demonstrate the influence of different levels (for low to high) of biogeochemical feedback sensitivity on future projections of wetland methane emissions. More specifically, we calculate emission changes from 2000 to 2100 (fig. S18) by assuming the response sensitivities of methane emissions to sulfate deposition and CO_2 enrichment at their 1st, 20th, 50th, 80th, and 99th percentile levels (fig. S17).

Supplementary Materials

The PDF file includes:

Supplementary Text S1 to S3
Figs. S1 to S29
Tables S1 to S6
Legends for data S1 to S3
References

Other Supplementary Material for this manuscript includes the following:

Data S1 to S3

REFERENCES AND NOTES

1. V. Naik, S. Szopa, B. Adhikary, P. Artaxo, T. Berntsen, W. D. Collins, S. Fuzzi, L. Gallardo, A. Kiendler Scharr, Z. Klimont, H. Liao, N. Unger, P. Zanis, "Short-lived climate forcers" in *Climate Change 2021: The Physical Science Basis. Contribution of Working Group I to the Sixth Assessment Report of the Intergovernmental Panel on Climate Change*, V. Masson- Delmotte, P. Zhai, A. Pirani, S. L. Connors, C. Péan, S. Berger, N. Caud, Y. Chen, L. Goldfarb, M. I. Gomis, M. Huang, K. Leitzell, E. Lonnoy, J. B. R. Matthews, T. K. Maycock, T. Waterfield, O. Yelekçi, R. Yu and B. Zhou, Eds. (Cambridge Univ. Press, 2021), pp. 817–922.
2. S. Kirschke, P. Bousquet, P. Ciais, M. Saunois, J. G. Canadell, E. J. Dlugokencky, P. Bergamaschi, D. Bergmann, D. R. Blake, L. Bruhwiler, P. Cameron-Smith, S. Castaldi, F. Chevallier, L. Feng, A. Fraser, M. Heimann, E. L. Hodson, S. Houweling, B. Josse, P. J. Fraser, P. B. Krummel, J.-F. Lamarque, R. L. Langenfelds, C. Le Quéré, V. Naik, S. O'Doherty, P. I. Palmer, I. Pison, D. Plummer, B. Poulter, R. G. Prinn, M. Rigby, B. Ringeval, M. Santini, M. Schmidt, D. T. Shindell, I. J. Simpson, R. Spahni, L. P. Steele, S. A. Strode, K. Sudo, S. Szopa, G. R. van der Werf, A. Voulgarakis, M. van Weele, R. F. Weiss, J. E. Williams, G. Zeng, Three decades of global methane sources and sinks. *Nat. Geosci.* **6**, 813–823 (2013).
3. M. Saunois, A. R. Stavert, B. Poulter, P. Bousquet, J. G. Canadell, R. B. Jackson, P. A. Raymond, E. J. Dlugokencky, S. Houweling, P. K. Patra, P. Ciais, V. K. Arora, D. Bastviken, P. Bergamaschi, D. R. Blake, G. Brailsford, L. Bruhwiler, K. M. Carlson, M. Carrol, S. Castaldi, N. Chandra, C. Crevoisier, P. M. Crill, K. Covey, C. L. Curry, G. Etiope, C. Frankenberg, N. Gedney, M. I. Hegglin, L. Höglund-Isaksson, G. Hugelius, M. Ishizawa, A. Ito, G. Janssens-Maenhout, K. M. Jensen, F. Joos, T. Kleinen, P. B. Krummel, R. L. Langenfelds, G. G. Laruelle, L. Liu, T. Machida, S. Maksyutov, K. C. McDonald, J. McNorton, P. A. Miller, J. R. Melton, I. Morino, J. Müller, F. Murguia-Flores, V. Naik, Y. Niwa, S. Noce, S. O'Doherty, R. J. Parker, C. Peng, S. Peng, G. P. Peters, C. Prigent, R. Prinn, M. Ramonet, P. Regnier, W. J. Riley, J. A. Rosentreter, A. Segers, I. J. Simpson, H. Shi, S. J. Smith, L. P. Steele, B. F. Thornton, H. Tian, Y. Tohjima, F. N. Tubiello, A. Tsuruta, N. Viovy, A. Voulgarakis, T. S. Weber, M. van Weele, G. R. van der Werf, R. F. Weiss, D. Worthy, D. Wunch, Y. Yin, Y. Yoshida, W. Zhang, Z. Zhang, Y. Zhao, B. Zheng, Q. Zhu, Q. Zhu, Q. Zhuang, The global methane budget 2000–2017. *Earth Syst. Sci. Data* **12**, 1561–1623 (2020).
4. S. Basu, X. Lan, E. Dlugokencky, S. Michel, S. Schwietzke, J. B. Miller, L. Bruhwiler, Y. Oh, P. P. Tans, F. Apadula, L. V. Gatti, A. Jordan, J. Necki, M. Sasakawa, S. Morimoto, T. Di Iorio, H. Lee, J. Arduini, G. Manca, Estimating emissions of methane consistent with atmospheric measurements of methane and δ^{13} C of methane. *Atmos. Chem. Phys.* **22**, 15351–15377 (2022).
5. M. Saunois, A. Martinez, B. Poulter, Z. Zhang, P. Raymond, P. Regnier, J. G. Canadell, R. B. Jackson, P. K. Patra, P. Bousquet, P. Ciais, E. J. Dlugokencky, X. Lan, G. H. Allen, D. Bastviken, D. J. Beerling, D. A. Belikov, D. R. Blake, S. Castaldi, M. Crippa, B. R. Deemer, F. Dennison, G. Etiope, N. Gedney, L. Höglund-Isaksson, M. A. Holgerson, P. O. Hopcroft, G. Hugelius, A. Ito, A. K. Jain, R. Janardanan, M. S. Johnson, T. Kleinen, P. Krummel, R. Lauerwald, T. Li, X. Liu, K. C. McDonald, J. R. Melton, J. Mühle, J. Müller, F. Murguia-Flores, Y. Niwa, S. Noce, S. Pan, R. J. Parker, C. Peng, M. Ramonet, W. J. Riley, G. Rocher-Ros, J. A. Rosentreter, M. Sasakawa, A. Segers, S. J. Smith, E. H. Stanley, J. Thanwerdas, H. Tian, A. Tsuruta, F. N. Tubiello, T. S. Weber, G. Van Der Werf, D. E. Worthy, Y. Xi, Y. Yoshida, W. Zhang, B. Zheng, Q. Zhu, Q. Zhu, Q. Zhuang, Global methane budget 2000–2020. *Earth Syst. Sci. Data Discuss.* , (2024). https://doi.org/10.5194/essd-2024-115.
6. E. G. Nisbet, E. J. Dlugokencky, M. R. Manning, D. Lowry, R. E. Fisher, J. L. France, S. E. Michel, J. B. Miller, J. W. C. White, B. Vaughn, P. Bousquet, J. A. Pyle, N. J. Warwick, M. Cain, R. Brownlow, G. Zazzeri, M. Lanoisellé, A. C. Manning, E. Gloor, D. E. J. Worthy, E.-G. Brunke, C. Labuschagne, E. W. Wolff, A. L. Ganesan, Rising atmospheric methane: 2007-2014 Growth and isotopic shift: RISING METHANE 2007–2014. *Global Biogeochem. Cycles* **30**, 1356–1370 (2016).
7. E. G. Nisbet, M. R. Manning, E. J. Dlugokencky, R. E. Fisher, D. Lowry, S. E. Michel, C. L. Myhre, S. M. Platt, G. Allen, P. Bousquet, R. Brownlow, M. Cain, J. L. France, O. Hermansen, R. Hossaini, A. E. Jones, I. Levin, A. C. Manning, G. Myhre, J. A. Pyle, B. H. Vaughn, N. J. Warwick, J. W. C. White, Very strong atmospheric methane growth in the 4 years 2014–2017: Implications for the Paris agreement. *Global Biogeochem. Cycles* **33**, 318–342 (2019).
8. E. G. Nisbet, M. R. Manning, E. J. Dlugokencky, S. E. Michel, X. Lan, T. Röckmann, H. A. C. Denier Van Der Gon, J. Schmitt, P. I. Palmer, M. N. Dyonisius, Y. Oh, R. E. Fisher, D. Lowry, J. L. France, J. W. C. White, G. Brailsford, T. Bromley, Atmospheric methane: Comparison between methane's record in 2006–2022 and during glacial terminations. *Global Biogeochem. Cycles* **37**, e2023GB007875 (2023).
9. X. Lan, S. Basu, S. Schwietzke, L. M. P. Bruhwiler, E. J. Dlugokencky, S. E. Michel, O. A. Sherwood, P. P. Tans, K. Thoning, G. Etiope, Q. Zhuang, L. Liu, Y. Oh, J. B. Miller, G. Pétron, B. H. Vaughn, M. Crippa, Improved constraints on global methane emissions and sinks using δ^{13} C-CH $_4$. *Global Biogeochem. Cycles* **35**, e2021GB007000 (2021).
10. Z. Zhang, B. Poulter, A. F. Feldman, Q. Ying, P. Ciais, S. Peng, X. Li, Recent intensification of wetland methane feedback. *Nat. Clim. Chang.* **13**, 430–433 (2023).
11. S. Peng, X. Lin, R. L. Thompson, Y. Xi, G. Liu, D. Hauglustaine, X. Lan, B. Poulter, M. Ramonet, M. Saunois, Y. Yin, Z. Zhang, B. Zheng, P. Ciais, Wetland emission and atmospheric sink changes explain methane growth in 2020. *Nature* **612**, 477–482 (2022).
12. Y. Oh, Q. Zhuang, L. R. Welp, L. Liu, X. Lan, S. Basu, E. J. Dlugokencky, L. Bruhwiler, J. B. Miller, S. E. Michel, S. Schwietzke, P. Tans, P. Ciais, J. P. Chanton, Improved global wetland carbon isotopic signatures support post-2006 microbial methane emission increase. *Commun Earth Environ* **3**, 159 (2022).
13. L. Feng, P. I. Palmer, R. J. Parker, M. F. Lunt, H. Bösch, Methane emissions are predominantly responsible for record-breaking atmospheric methane growth rates in 2020 and 2021. *Atmos. Chem. Phys.* **23**, 4863–4880 (2023).
14. A. Drinkwater, P. I. Palmer, L. Feng, T. Arnold, X. Lan, S. E. Michel, R. Parker, H. Boesch, Atmospheric data support a multi-decadal shift in the global methane budget towards natural tropical emissions. *Atmos. Chem. Phys.* **23**, 8429–8452 (2023).
15. Y. Zhu, K. J. Purdy, Ö. Eyice, L. Shen, S. F. Harpenslager, G. Yvon-Durocher, A. J. Dumbrell, M. Trimmer, Disproportionate increase in freshwater methane emissions induced by experimental warming. *Nat. Clim. Chang.* **10**, 685–690 (2020).
16. V. Gauci, E. Matthews, N. Dise, B. Walter, D. Koch, G. Granberg, M. Vile, Sulfur pollution suppression of the wetland methane source in the 20th and 21st centuries. *Proc. Natl. Acad. Sci. U.S.A.* **101**, 12583–12587 (2004).

Downloaded from https://www.science.org at Peking University on February 11, 2025

17. K. J. van Groenigen, C. W. Osenberg, B. A. Hungate, Increased soil emissions of potent greenhouse gases under increased atmospheric CO_2. *Nature* **475**, 214–216 (2011).
18. E. N. Koffi, P. Bergamaschi, R. Alkama, A. Cescatti, An observation-constrained assessment of the climate sensitivity and future trajectories of wetland methane emissions. *Sci. Adv.* **6**, eaay4444 (2020).
19. Z. Zhang, N. E. Zimmermann, A. Stenke, X. Li, E. L. Hodson, G. Zhu, C. Huang, B. Poulter, Emerging role of wetland methane emissions in driving 21st century climate change. *Proc. Natl. Acad. Sci. U.S.A.* **114**, 9647–9652 (2017).
20. N. Gedney, C. Huntingford, E. Comyn-Platt, A. Wiltshire, Significant feedbacks of wetland methane release on climate change and the causes of their uncertainty. *Environ. Res. Lett.* **14**, 084027 (2019).
21. A. V. Eliseev, I. I. Mokhov, M. M. Arzhanov, P. F. Demchenko, S. N. Denisov, Interaction of the methane cycle and processes in wetland ecosystems in a climate model of intermediate complexity. *Izv. Atmos. Ocean. Phys.* **44**, 139–152 (2008).
22. D. T. Shindell, B. P. Walter, G. Faluvegi, Impacts of climate change on methane emissions from wetlands. *Geophys. Res. Lett.* **31**, L21202 (2004).
23. N. Gedney, Climate feedback from wetland methane emissions. *Geophys. Res. Lett.* **31**, L20503 (2004).
24. B. D. Stocker, R. Roth, F. Joos, R. Spahni, M. Steinacher, S. Zaehle, L. Bouwman, Xu-Ri, I. C. Prentice, Multiple greenhouse-gas feedbacks from the land biosphere under future climate change scenarios. *Nat. Clim. Change* **3**, 666–672 (2013).
25. E. Comyn-Platt, G. Hayman, C. Huntingford, S. E. Chadburn, E. J. Burke, A. B. Harper, W. J. Collins, C. P. Webber, T. Powell, P. M. Cox, N. Gedney, S. Sitch, Carbon budgets for 1.5 and 2 °C targets lowered by natural wetland and permafrost feedbacks. *Nat. Geosci.* **11**, 568–573 (2018).
26. C. Gudasz, D. Bastviken, K. Steger, K. Premke, S. Sobek, L. J. Tranvik, Temperature-controlled organic carbon mineralization in lake sediments. *Nature* **466**, 478–481 (2010).
27. G. Yvon-Durocher, A. P. Allen, D. Bastviken, R. Conrad, C. Gudasz, A. St-Pierre, N. Thanh-Duc, P. A. del Giorgio, Methane fluxes show consistent temperature dependence across microbial to ecosystem scales. *Nature* **507**, 488–491 (2014).
28. S. E. Chadburn, T. Aalto, M. Aurela, D. Baldocchi, C. Biasi, J. Boike, E. J. Burke, E. Comyn-Platt, A. J. Dolman, C. Duran-Rojas, Y. Fan, T. Friborg, Y. Gao, N. Gedney, M. Göckede, G. D. Hayman, D. Holl, G. Hugelius, L. Kutzbach, H. Lee, A. Lohila, F. W. Parmentier, T. Sachs, N. J. Shurpali, S. Westermann, Modeled microbial dynamics explain the apparent temperature sensitivity of wetland methane emissions. *Global Biogeochem. Cycles* **34**, e2020GB006678 (2020).
29. Y. Hu, X. Yue, C. Tian, H. Zhou, W. Fu, X. Zhao, Y. Zhao, Y. Chen, Identifying the main drivers of the spatiotemporal variations in wetland methane emissions during 2001–2020. *Front. Environ. Sci.* **11**, 1275742 (2023).
30. E. G. Nisbet, Climate feedback on methane from wetlands. *Nat. Clim. Chang.* **13**, 421–422 (2023).
31. W. J. Riley, Z. M. Subin, D. M. Lawrence, S. C. Swenson, M. S. Torn, L. Meng, N. M. Mahowald, P. Hess, Barriers to predicting changes in global terrestrial methane fluxes: Analyses using CLM4Me, a methane biogeochemistry model integrated in CESM. *Biogeosciences* **8**, 1925–1953 (2011).
32. X. Xu, F. Yuan, P. J. Hanson, S. D. Wullschleger, P. E. Thornton, W. J. Riley, X. Song, D. E. Graham, C. Song, H. Tian, Reviews and syntheses: Four decades of modeling methane cycling in terrestrial ecosystems. *Biogeosciences* **13**, 3735–3755 (2016).
33. H. Chen, X. Xu, C. Fang, B. Li, M. Nie, Differences in the temperature dependence of wetland CO_2 and CH4 emissions vary with water table depth. *Nat. Clim. Chang.* **11**, 766–771 (2021).
34. F. Murguia-Flores, V. J. Jaramillo, A. Gallego-Sala, Assessing methane emissions from tropical wetlands: Uncertainties from natural variability and drivers at the global scale. *Glob. Biogeochem.l Cycles* **37**, e2022GB007601 (2023).
35. E. M. Volodin, Methane cycle in the INM RAS climate model. *Izv. Atmos. Ocean. Phys.* **44**, 153–159 (2008).
36. D. R. Lovley, M. J. Klug, Sulfate reducers can outcompete methanogens at freshwater sulfate concentrations. *Appl. Environ. Microbiol.* **45**, 187–192 (1983).
37. M. R. Winfrey, J. G. Zeikus, Effect of sulfate on carbon and electron flow during microbial methanogenesis in freshwater sediments. *Appl. Environ. Microbiol.* **33**, 275–281 (1977).
38. P. Durack, K. Taylor, V. Eyring, S. Ames, C. Doutriaux, T. Hoang, D. Nadeau, M. Stockhause, P. Gleckler, "input4MIPs: Making [CMIP] model forcing more transparent" (LLNL-JRNL-729886, 1463030, 880514, 2017); https://doi.org/10.2172/1463030.
39. L. Deng, C. Huang, D. Kim, Z. Shangguan, K. Wang, X. Song, C. Peng, Soil GHG fluxes are altered by N deposition: New data indicate lower N stimulation of the N_2O flux and greater stimulation of the calculated C pools. *Glob Change Biol* **26**, 2613–2629 (2020).
40. J. Wu, X. Cheng, W. Xing, G. Liu, Soil-atmosphere exchange of CH4 in response to nitrogen addition in diverse upland and wetland ecosystems: A meta-analysis. *Soil Biol. Biochem.* **164**, 108467 (2022).
41. K. Banger, H. Tian, C. Lu, Do nitrogen fertilizers stimulate or inhibit methane emissions from rice fields? *Glob. Change Biol.* **18**, 3259–3267 (2012).
42. J. W. H. Dacey, B. G. Drake, M. J. Klug, Stimulation of methane emission by carbon dioxide enrichment of marsh vegetation. *Nature* **370**, 47–49 (1994).
43. Y. Lin, J. Yuan, D. Liu, H. Kang, C. Freeman, H.-W. Hu, G. Ye, W. Ding, Divergent responses of wetland methane emissions to elevated atmospheric CO_2 dependent on water table. *Water Res.* **205**, 117682 (2021).
44. H. Qian, Y. Jin, J. Chen, S. Huang, Y. Liu, J. Zhang, A. Deng, J. Zou, G. Pan, Y. Ding, Y. Jiang, K. J. van Groenigen, W. Zhang, Acclimation of CH4 emissions from paddy soil to atmospheric CO_2 enrichment in a growth chamber experiment. *Crop J* **10**, 140–146 (2022).
45. L. Möller, T. Sowers, M. Bock, R. Spahni, M. Behrens, J. Schmitt, H. Miller, H. Fischer, Independent variations of CH4 emissions and isotopic composition over the past 160,000 years. *Nat. Geosci.* **6**, 885–890 (2013).
46. W. J. Collins, J.-F. Lamarque, M. Schulz, O. Boucher, V. Eyring, M. I. Hegglin, A. Maycock, G. Myhre, M. Prather, D. Shindell, S. J. Smith, AerChemMIP: Quantifying the effects of chemistry and aerosols in CMIP6. *Geosci. Model Dev.* **10**, 585–607 (2017).
47. M. Meinshausen, Z. R. J. Nicholls, J. Lewis, M. J. Gidden, E. Vogel, M. Freund, U. Beyerle, C. Gessner, A. Nauels, N. Bauer, J. G. Canadell, J. S. Daniel, A. John, P. B. Krummel, G. Luderer, N. Meinshausen, S. A. Montzka, P. J. Rayner, S. Reimann, S. J. Smith, M. van den Berg, G. J. M. Velders, M. K. Vollmer, R. H. J. Wang, The shared socio-economic pathway (SSP) greenhouse gas concentrations and their extensions to 2500. *Geosci. Model Dev.* **13**, 3571–3605 (2020).
48. W. Cheng, L. Dan, X. Deng, J. Feng, Y. Wang, J. Peng, J. Tian, W. Qi, Z. Liu, X. Zheng, D. Zhou, S. Jiang, H. Zhao, X. Wang, Global monthly gridded atmospheric carbon dioxide concentrations under the historical and future scenarios. *Sci. Data* **9**, 83 (2022).
49. A. A. Bloom, K. W. Bowman, M. Lee, A. J. Turner, R. Schroeder, J. R. Worden, R. Weidner, K. C. McDonald, D. J. Jacob, A global wetland methane emissions and uncertainty dataset for atmospheric chemical transport models (WetCHARTs version 1.0). *Geosci. Model Dev.* **10**, 2141–2156 (2017).
50. S. Ma, J. R. Worden, A. A. Bloom, Y. Zhang, B. Poulter, D. H. Cusworth, Y. Yin, S. Pandey, J. D. Maasakkers, X. Lu, L. Shen, J. Sheng, C. Frankenberg, C. E. Miller, D. J. Jacob, Satellite constraints on the latitudinal distribution and temperature sensitivity of wetland methane emissions. *AGU Adv.* **2**, e2021AV000408 (2021).
51. L. Shen, D. J. Jacob, R. Gautam, M. Omara, T. R. Scarpelli, A. Lorente, D. Zavala-Araiza, X. Lu, Z. Chen, J. Lin, National quantifications of methane emissions from fuel exploitation using high resolution inversions of satellite observations. *Nat. Commun.* **14**, 4948 (2023).
52. B. Zhang, H. Tian, C. Lu, G. Chen, S. Pan, C. Anderson, B. Poulter, Methane emissions from global wetlands: An assessment of the uncertainty associated with various wetland extent data sets. *Atmos. Environ.* **165**, 310–321 (2017).
53. C. Gerlein-Safdi, A. A. Bloom, G. Plant, E. A. Kort, C. S. Ruf, Improving representation of tropical wetland methane emissions with CYGNSS inundation maps. *Global Biogeochem. Cycles* **35**, e2020GB006890 (2021).
54. S. Calabrese, A. Garcia, J. L. Wilmoth, X. Zhang, A. Porporato, Critical inundation level for methane emissions from wetlands. *Environ. Res. Lett.* **16**, 044038 (2021).
55. K. Chang, W. J. Riley, N. Collier, G. McNicol, E. Fluet-Chouinard, S. H. Knox, K. B. Delwiche, R. B. Jackson, B. Poulter, M. Saunois, N. Chandra, N. Gedney, M. Ishizawa, A. Ito, F. Joos, T. Kleinen, F. Maggi, J. McNorton, J. R. Melton, P. Miller, Y. Niwa, C. Pasut, P. K. Patra, C. Peng, S. Peng, A. Segers, H. Tian, A. Tsuruta, Y. Yao, Y. Yin, W. Zhang, Z. Zhang, Q. Zhu, Q. Zhu, Q. Zhuang, Observational constraints reduce model spread but not uncertainty in global wetland methane emission estimates. *Glob. Change Biol.* **29**, 4298–4312 (2023).
56. V. Gauci, V. Figueiredo, N. Gedney, S. R. Pangala, T. Stauffer, G. P. Weedon, A. Enrich-Prast, Non-flooded riparian Amazon trees are a regionally significant methane source. *Phil. Trans. R. Soc. A.* **380**, 20200446 (2022).
57. J. T. Shaw, G. Allen, P. Barker, J. R. Pitt, D. Pasternak, S. J.-B. Bauguitte, J. Lee, K. N. Bower, M. C. Daly, M. F. Lunt, A. L. Ganesan, A. R. Vaughan, F. Chibesakunda, M. Lambakasa, R. E. Fisher, J. L. France, D. Lowry, P. I. Palmer, S. Metzger, R. J. Parker, N. Gedney, P. Bateson, M. Cain, A. Lorente, T. Borsdorff, E. G. Nisbet, Large methane emission fluxes observed from tropical wetlands in Zambia. *Global Biogeochem. Cycles* **36**, e2021GB007261 (2022).
58. G. Muyzer, A. J. M. Stams, The ecology and biotechnology of sulphate-reducing bacteria. *Nat. Rev. Microbiol.* **6**, 441–454 (2008).
59. C. P. Boardman, V. Gauci, A. Fox, S. Blake, D. J. Beerling, Reduction of the temperature sensitivity of minerotrophic fen methane emissions by simulated glacial atmospheric carbon dioxide starvation. *J. Geophys. Res. Biogeosci.* **118**, 462–470 (2013).
60. J. Ehleringer, O. Björkman, Quantum yields for CO_2 uptake in C_3 and C_4 plants: Dependence on temperature, CO_2, and O_2 concentration. *Plant Physiol.* **59**, 86–90 (1977).
61. R. F. Sage, D. S. Kubien, The temperature response of C_3 and C_4 photosynthesis. *Plant Cell Environ.* **30**, 1086–1106 (2007).
62. C. J. Still, J. A. Berry, G. J. Collatz, R. S. DeFries, Global distribution of C_3 and C_4 vegetation: Carbon cycle implications. *Global Biogeochem. Cycles* **17**, 6.1–6.14 (2003).
63. E. J. Burke, Y. Zhang, G. Krinner, Evaluating permafrost physics in the Coupled Model Intercomparison Project 6 (CMIP6) models and their sensitivity to climate change. *Cryosphere* **14**, 3155–3174 (2020).
64. G. J. Collatz, J. A. Berry, J. S. Clark, Effects of climate and atmospheric CO_2 partial pressure on the global distribution of C 4 grasses: Present, past, and future. *Oecologia* **114**, 441–454 (1998).

Downloaded from https://www.science.org at Peking University on February 11, 2025

65. J. A. Morgan, D. R. LeCain, E. Pendall, D. M. Blumenthal, B. A. Kimball, Y. Carrillo, D. G. Williams, J. Heisler-White, F. A. Dijkstra, M. West, C_4 grasses prosper as carbon dioxide eliminates desiccation in warmed semi-arid grassland. *Nature* **476**, 202–205 (2011).
66. T. Weber, N. A. Wiseman, A. Kock, Global ocean methane emissions dominated by shallow coastal waters. *Nat. Commun.* **10**, 4584 (2019).
67. R. A. Alvarez, D. Zavala-Araiza, D. R. Lyon, D. T. Allen, Z. R. Barkley, A. R. Brandt, K. J. Davis, S. C. Herndon, D. J. Jacob, A. Karion, E. A. Kort, B. K. Lamb, T. Lauvaux, J. D. Maasakkers, A. J. Marchese, M. Omara, S. W. Pacala, J. Peischl, A. L. Robinson, P. B. Shepson, C. Sweeney, A. Townsend-Small, S. C. Wofsy, S. P. Hamburg, Assessment of methane emissions from the U.S. oil and gas supply chain. *Science* **361**, 186–188 (2018).
68. T. R. Scarpelli, D. J. Jacob, S. Grossman, X. Lu, Z. Qu, M. P. Sulprizio, Y. Zhang, F. Reuland, D. Gordon, J. R. Worden, Updated Global Fuel Exploitation Inventory (GFEI) for methane emissions from the oil, gas, and coal sectors: Evaluation with inversions of atmospheric methane observations. *Atmos. Chem. Phys.* **22**, 3235–3249 (2022).
69. European Commission and USA, About the Global Methane Pledge (2021), www.globalmethanepledge.org [accessed December 2023].
70. V. Gauci, N. Dise, S. Blake, Long-term suppression of wetland methane flux following a pulse of simulated acid rain. *Geophys. Res. Lett.* **32**, L12804 (2005).
71. M. Guimberteau, D. Zhu, F. Maignan, Y. Huang, C. Yue, S. Dantec-Nédélec, C. Ottlé, A. Jornet-Puig, A. Bastos, P. Laurent, D. Goll, S. Bowring, J. Chang, B. Guenet, M. Tifafi, S. Peng, G. Krinner, A. Ducharne, F. Wang, T. Wang, X. Wang, Y. Wang, Z. Yin, R. Lauerwald, E. Joetzjer, C. Qiu, H. Kim, P. Ciais, ORCHIDEE-MICT (v8.4.1), a land surface model for the high latitudes: Model description and validation. *Geosci. Model Dev.* **11**, 121–163 (2018).
72. T. F. Keenan, X. Luo, B. D. Stocker, M. G. De Kauwe, B. E. Medlyn, I. C. Prentice, N. G. Smith, C. Terrer, H. Wang, Y. Zhang, S. Zhou, A constraint on historic growth in global photosynthesis due to rising CO2. *Nat. Clim. Chang.* **13**, 1376–1381 (2023).
73. H. A. Denier Van Der Gon, P. M. Van Bodegom, R. Wassmann, R. S. Lantin, T. M. Metra-Corton, Sulfate-containing amendments to reduce methane emissions from rice fields: Mechanisms, effectiveness and costs. *Mitig. Adapt. Strat. Glob. Chang.* **6**, 71–89 (2001).
74. V. Gauci, N. B. Dise, G. Howell, M. E. Jenkins, Suppression of rice methane emission by sulfate deposition in simulated acid rain. *J. Geophys. Res.* **113**, 2007JG000501 (2008).
75. E. Salmon, F. Jégou, B. Guenet, L. Jourdain, C. Qiu, V. Bastrikov, C. Guimbaud, D. Zhu, P. Ciais, P. Peylin, S. Gogo, F. Laggoun-Défarge, M. Aurela, M. S. Bret-Harte, J. Chen, B. H. Chojnicki, H. Chu, C. W. Edgar, E. S. Euskirchen, L. B. Flanagan, K. Fortuniak, D. Holl, J. Klatt, O. Kolle, N. Kowalska, L. Kutzbach, A. Lohila, L. Merbold, W. Pawlak, T. Sachs, K. Ziemblińska, Assessing methane emissions for northern peatlands in ORCHIDEE-PEAT revision 7020. *Geosci. Model Dev.* **15**, 2813–2838 (2022).
76. P. Bergamaschi, S. Houweling, A. Segers, M. Krol, C. Frankenberg, R. A. Scheepmaker, E. Dlugokencky, S. C. Wofsy, E. A. Kort, C. Sweeney, T. Schuck, C. Brenninkmeijer, H. Chen, V. Beck, C. Gerbig, Atmospheric CH_4 in the first decade of the 21st century: Inverse modeling analysis using SCIAMACHY satellite retrievals and NOAA surface measurements. *J. Geophys. Res. Atmos.* **118**, 7350–7369 (2013).
77. R. Gelaro, W. McCarty, M. J. Suárez, R. Todling, A. Molod, L. Takacs, C. A. Randles, A. Darmenov, M. G. Bosilovich, R. Reichle, K. Wargan, L. Coy, R. Cullather, C. Draper, S. Akella, V. Buchard, A. Conaty, A. M. Da Silva, W. Gu, G.-K. Kim, R. Koster, R. Lucchesi, D. Merkova, J. E. Nielsen, G. Partyka, S. Pawson, W. Putman, M. Rienecker, S. D. Schubert, M. Sienkiewicz, B. Zhao, The modern-era retrospective analysis for research and applications, version 2 (MERRA-2). *J. Climate* **30**, 5419–5454 (2017).
78. S. E. Nicholson, Long-term variability of the East African 'short rains' and its links to large-scale factors. *Intl Journal of Climatology* **35**, 3979–3990 (2015).
79. S. Pandey, S. Houweling, M. Krol, I. Aben, G. Monteil, N. Nechita-Banda, E. J. Dlugokencky, R. Detmers, O. Hasekamp, X. Xu, W. J. Riley, B. Poulter, Z. Zhang, K. C. McDonald, J. W. C. White, P. Bousquet, T. Röckmann, Enhanced methane emissions from tropical wetlands during the 2011 La Niña. *Sci. Rep.* **7**, 45759 (2017).
80. V. Eyring, S. Bony, G. A. Meehl, C. A. Senior, B. Stevens, R. J. Stouffer, K. E. Taylor, Overview of the Coupled Model Intercomparison Project Phase 6 (CMIP6) experimental design and organization. *Geosci. Model Dev.* **9**, 1937–1958 (2016).
81. L. Shen, L. J. Mickley, L. T. Murray, Influence of 2000–2050 climate change on particulate matter in the United States: Results from a new statistical model. *Atmos. Chem. Phys.* **17**, 4355–4367 (2017).
82. Z. Zhang, E. Fluet-Chouinard, K. Jensen, K. McDonald, G. Hugelius, T. Gumbricht, M. Carroll, C. Prigent, A. Bartsch, B. Poulter, Development of the global dataset of Wetland Area and Dynamics for Methane Modeling (WAD2M). *Earth Syst. Sci. Data* **13**, 2001–2023 (2021).
83. G. McNicol, E. Fluet-Chouinard, Z. Ouyang, S. Knox, Z. Zhang, T. Aalto, S. Bansal, K. Chang, M. Chen, K. Delwiche, S. Feron, M. Goeckede, J. Liu, A. Malhotra, J. R. Melton, W. Riley, R. Vargas, K. Yuan, Q. Ying, Q. Zhu, P. Alekseychik, M. Aurela, D. P. Billesbach, D. I. Campbell, J. Chen, H. Chu, A. R. Desai, E. Euskirchen, J. Goodrich, T. Griffis, M. Helbig, T. Hirano, H. Iwata, G. Jurasinski, J. King, F. Koebsch, R. Kolka, K. Krauss, A. Lohila, I. Mammarella, M. Nilson, A. Noormets, W. Oechel, M. Peichl, T. Sachs, A. Sakabe, C. Schulze, O. Sonnentag, R. C. Sullivan, E. Tuittila, M. Ueyama, T. Vesala, E. Ward, C. Wille, G. X. Wong, D. Zona, L. Windham-Myers, B. Poulter, R. B. Jackson, Upscaling wetland methane emissions from the FLUXNET-CH4 Eddy covariance network (UpCH4 v1.0): Model development, network assessment, and budget comparison. *AGU Adv.* **4**, e2023AV000956 (2023).
84. M. J. Gidden, K. Riahi, S. J. Smith, S. Fujimori, G. Luderer, E. Kriegler, D. P. van Vuuren, M. van den Berg, L. Feng, D. Klein, K. Calvin, J. C. Doelman, S. Frank, O. Fricko, M. Harmsen, T. Hasegawa, P. Havlik, J. Hilaire, R. Hoesly, J. Horing, A. Popp, E. Stehfest, K. Takahashi, Global emissions pathways under different socioeconomic scenarios for use in CMIP6: A dataset of harmonized emissions trajectories through the end of the century. *Geosci. Model Dev.* **12**, 1443–1475 (2019).
85. A. J. Cannon, S. R. Sobie, T. Q. Murdock, Bias correction of gcm precipitation by quantile mapping: How well do methods preserve changes in quantiles and extremes? *J. Climate* **28**, 6938–6959 (2015).
86. IPCC, *Climate Change 2021: The Physical Science Basis. Contribution of Working Group I to the Sixth Assessment Report of the Intergovernmental Panel on Climate Change*, V. Masson-Delmotte, P. Zhai, A. Pirani, S. L. Connors, C. Péan, S. Berger, N. Caud, Y. Chen, L. Goldfarb, M. I. Gomis, M. Huang, K. Leitzell, E. Lonnoy, J. B. R. Matthews, T. K. Maycock, T. Waterfield, O. Yelekçi, R. Yu and B. Zhou, Eds. (Cambridge Univ. Press, 2021).
87. M. Pester, Sulfate-reducing microorganisms in wetlands – fameless actors in carbon cycling and climate change. *Front. Microbio.* **3**, 72 (2012).
88. A. J. M. Stams, S. J. W. H. O. Elferink, P. Westermann, "Metabolic Interactions Between Methanogenic Consortia and Anaerobic Respiring Bacteria" in *Biomethanation I*, B. K. Ahring, I. Angelidaki, E. C. de Macario, H. N. Gavala, J. Hofman-Bang, A. J. L. Macario, S. J. W. H. O. Elferink, L. Raskin, A. J. M. Stams, P. Westermann, D. Zheng, Eds. (Springer, 2003), pp. 31–56.
89. R. Wania, J. R. Melton, E. L. Hodson, B. Poulter, B. Ringeval, R. Spahni, T. Bohn, C. A. Avis, G. Chen, A. V. Eliseev, P. O. Hopcroft, W. J. Riley, Z. M. Subin, H. Tian, P. M. van Bodegom, T. Kleinen, Z. C. Yu, J. S. Singarayer, S. Zürcher, D. P. Lettenmaier, D. J. Beerling, S. N. Denisov, C. Prigent, F. Papa, J. O. Kaplan, Present state of global wetland extent and wetland methane modelling: Methodology of a model inter-comparison project (WETCHIMP). *Geosci. Model Dev.* **6**, 617–641 (2013).
90. D. Yan, K. Wang, T. Qin, B. Weng, H. Wang, W. Bi, X. Li, M. Li, Z. Lv, F. Liu, S. He, J. Ma, Z. Shen, J. Wang, H. Bai, Z. Man, C. Sun, M. Liu, X. Shi, L. Jing, R. Sun, S. Cao, C. Hao, L. Wang, M. Pei, B. Dorjsuren, M. Gedefaw, A. Girma, A. Abiyu, A data set of global river networks and corresponding water resources zones divisions. *Sci. Data* **6**, 219 (2019).
91. A. L. Ganesan, A. C. Stell, N. Gedney, E. Comyn-Platt, G. Hayman, M. Rigby, B. Poulter, E. R. C. Hornibrook, Spatially resolved isotopic source signatures of wetland methane emissions. *Geophys. Res. Lett.* **45**, 3737–3745 (2018).
92. B. Ringeval, P. Friedlingstein, C. Koven, P. Ciais, N. de Noblet-Ducoudré, B. Decharme, P. Cadule, Climate-CH_4 feedback from wetlands and its interaction with the climate-CO_2 feedback. *Biogeosciences* **8**, 2137–2157 (2011).
93. M. J. Prather, C. D. Holmes, J. Hsu, Reactive greenhouse gas scenarios: Systematic exploration of uncertainties and the role of atmospheric chemistry. *Geophys. Res. Lett.* **39**, 2012GL051440 (2012).
94. United Nations Environment Programme and Climate and Clean Air Coalition, "Global methane assessment: Benefits and costs of mitigating methane emissions" (Publication 978-92-807-3854-4, 2021); https://wedocs.unep.org/bitstream/handle/20.500.11822/35913/GMA.pdf.

Acknowledgments

Funding: Work at Peking University was supported by the National Natural Science Foundation of China (42275194, L.S.) and the National Key Research and Development Program of China (2023YFC3707404, L.S.). **Author contributions:** Conceptualization: LS. Methodology: L.S., S.P., and V.G. Investigation: L.S., S.P., and Z.Z. Visualization: L.S., C.T., J.L., Y.L., H.Z., and S.M. Writing—original draft: L.S. Writing—review and editing: L.S., S.P., V.G., Y.L., and M.Z. **Competing interests:** The authors declare that they have no competing interests. **Data and materials availability:** All data needed to evaluate the conclusions in the paper are present in the paper and/or the Supplementary Materials. The data of Coupled Model Intercomparison Project phase 6 (CMIP6), including projections of meteorological data and sulfate deposition, can be downloaded at https://esgf-node.llnl.gov/projects/cmip6/. All data and codes generated in this study are available at https://doi.org/10.18170/DVN/ZLEPKQ.

Submitted 27 November 2023
Accepted 6 January 2025
Published 5 February 2025
10.1126/sciadv.adn1056

Downloaded from https://www.science.org at Peking University on February 11, 2025